doi:10.1093/brain/awx046 BRAIN 2017: 140; 1499–1512 | 1499

BRAIN
A JOURNAL OF NEUROLOGY

Association between tau deposition and antecedent amyloid-β accumulation rates in normal and early symptomatic individuals

Duygu Tosun,[1] Susan Landau,[2] Paul S. Aisen,[3] Ronald C. Petersen,[4] Mark Mintun,[5] William Jagust[2] and Michael W. Weiner[1] for the Alzheimer's Disease Neuroimaging Initiative

See Vandenberghe and Schaeverbeke (doi:10.1093/awx065) for a scientific commentary on this article.

A long-term goal of our field is to determine the sequence of pathological events, which ultimately lead to cognitive decline and dementia. In this study, we first assessed the patterns of brain tau tangle accumulation (measured with the positron emission tomography tracer ^{18}F-AV-1451) associated with well-established Alzheimer's disease factors in a cohort including cognitively healthy elderly individuals and individuals at early symptomatic stages of Alzheimer's disease. We then explored highly associated patterns of greater ^{18}F-AV-1451 binding and increased annualized change in cortical amyloid-β plaques measured as florbetapir positron emission tomography binding antecedent to ^{18}F-AV-1451 positron emission tomography scans, and to what extent these multimodal pattern associations explained the variance in cognitive performance and clinical outcome measures, independently and jointly. We found that: (i) ^{18}F-AV-1451 positron emission tomography retention was differentially associated with age, and cross-sectional florbetapir positron emission tomography retention, but not with years of education, gender, or *APOE* genotype; (ii) increased annualized change in florbetapir retention, antecedent to ^{18}F-AV-1451 positron emission tomography scans, in the parieto-temporal and precuneus brain regions was associated with greater ^{18}F-AV-1451 PET retention most prominently in the inferior temporal and inferior parietal regions in the full cohort, with florbetapir positive/negative-associated variability; and (iii) this ^{18}F-AV-1451 positron emission tomography retention pattern significantly explained the variance in cognitive performance and clinical outcome measures, independent of the associated antecedent increased annualized change in florbetapir positron emission tomography retention. These findings are in agreement with the pathology literature, which suggests that tau tangles but not amyloid-β plaques correlate with cognition and clinical symptoms. Furthermore, non-local associations linking increased amyloid-β accumulation rates with increased tau deposition are of great interest and support the idea that the amyloid-β pathology might have remote effects in disease pathology spread potentially via the brain's intrinsic connectivity networks.

1 Department of Radiology and Biomedical Imaging, University of California – San Francisco, San Francisco, CA, USA
2 Helen Wills Neuroscience Institute, University of California, Berkeley, CA, USA
3 Department of Neurology, University of California-San Diego, San Diego, CA, USA
4 Department of Neurology, Mayo Clinic, Rochester MN, USA
5 Avid Radiopharmaceuticals, Philadelphia, PA, USA

Correspondence to: Duygu Tosun, PhD,
Department of Radiology and Biomedical Imaging University of California – San Francisco
4150 Clement St, Bldg 13, 114M
San Francisco, CA 94121, USA
E-mail: duygu.tosun@ucsf.edu

Received May 31, 2016. Revised December 12, 2016. Accepted January 17, 2017. Advance Access publication March 17, 2017.

Keywords: amyloid-β; tau; positron emission tomography; Alzheimer's disease

Abbreviations: CDR-SB = Clinical Dementia Rating-Sum of Boxes; MCI = mild cognitive impairment; MMSE = Mini-Mental State Examination; SUVR = standardized uptake value ratio

Introduction

Alzheimer's disease is associated with widespread deposition of extracellular amyloid-β peptides into cortical amyloid-β plaques and deposition of intracellular phosphorylated tau protein into neurofibrillary tangles in disease-specific brain regions (Hyman and Trojanowski, 1997). Braak (Braak *et al.*, 2011) and others (Braak and Braak, 1996; Bradley *et al.*, 2002; Vemuri *et al.*, 2008), using neuropathology, demonstrated a close correlation between tau tangles and neurodegeneration. Furthermore, the neuropathology literature suggests that tau tangles, but not amyloid-β plaques, correlate with cognition (Markesbery, 1997), especially memory function (Terry *et al.*, 1999), which characterizes Alzheimer's disease. Therefore, tau tangle-associated neurodegeneration is likely to be part of the chain of events leading to cortical dysfunction and cognitive impairment. Yet, the neuropathology literature concerning the distribution of amyloid-β, tau, and their relationship to cognition is complex (Terry and Katzman, 1983; Price, 1997; Berg *et al.*, 1998), reporting cases with little amyloid-β and tau in young subjects, cases with widespread amyloid-β plaques but without tau tangles (Tiraboschi *et al.*, 2004; Nelson *et al.*, 2009), cases with tau tangles in the absence of amyloid-β plaques (Nelson *et al.*, 2009), and cases with both amyloid-β plaques and tau tangles widely distributed, especially as seen in subjects with dementia due to Alzheimer's disease (Knopman *et al.*, 2003; Monsell *et al.*, 2013). One well-established finding from neuropathological studies is the existence of intracellular tau tangles in non-demented cases, especially in the earliest tau tangle formation brain sites including transentorhinal cortex, entorhinal cortex, and hippocampus (Price and Morris, 1999). Furthermore, the neuropathology studies report exponential increase in the concentration of tau tangles with age, and greater spatial spread and further increase in concentration in the presence of widely distributed neuritic as well as diffuse plaques throughout neocortex and limbic structures (Price and Morris, 1999). These reports suggest an interaction between the pace of amyloid-β deposition and the spread of tau tangles, even at the earliest disease stage. However, limitations of pathology studies are that they only represent one time point, that the brain specimens are collected at some considerable time from the previous clinical evaluation, and that different studies use different methods, making a consensus view of the chain of events in living humans difficult to achieve.

In-depth analysis of the cause-effect mechanisms by which amyloid-β, tau, and symptomatology interact is of great interest, particularly for development of therapeutic strategies for Alzheimer's disease. The amyloid-β cascade hypothesis (Hardy and Selkoe, 2002; Karran *et al.*, 2011), the prevailing hypothesis in Alzheimer's disease research, posits that accumulation of amyloid-β is primarily responsible for the accumulation of tau tangles, synaptic dysfunction, neurodegeneration, and cognitive decline especially in memory function. In addition to the knowledge gained from aforementioned neuropathology studies, accumulating evidence from *in vitro* tissue experiments and *in vivo* animal models has also provided direct experimental support for the amyloid-β cascade hypothesis, particularly for the amyloid-β-induced tau accumulation (Hurtado *et al.*, 2010; Pooler *et al.*, 2015). Most importantly, recently developed PET ligands for amyloid-β (Mintun *et al.*, 2006; Clark *et al.*, 2011) and tau (Fodero-Tavoletti *et al.*, 2011; Xia *et al.*, 2013) provide information concerning the amount and topography of deposition of these two hallmark pathologies of Alzheimer's disease *in vivo*. These PET ligands will enable temporal and spatial localization of the amyloid-β and tau, their respective contribution to the aetiology of Alzheimer's disease, and the mechanistic link between amyloid-β and tau pathology examined *in vivo* for the first time. Here, we examined *in vivo* the burden and the anatomical distribution of tau pathology as measured by ^{18}F-AV-1451 PET retention (Xia *et al.*, 2013) and its relationship with antecedent and cross-sectional amyloid-β pathology as measured by florbetapir-PET retention longitudinally (Wong *et al.*, 2010), as well as its relationship with other Alzheimer's disease-related factors, using data from asymptomatic elderly individuals and early symptomatic individuals, recruited in a multi-centre Alzheimer's Disease Neuroimaging Initiative (ADNI) study. Alzheimer's disease-related factors considered in this study were limited to age, gender, education, and *APOE* genotype based on the current literature reporting associations between these factors and neurobiological factors implicated in Alzheimer's disease. Specifically, after advanced age, *APOE* ε4 genotype is a major risk factor for developing Alzheimer's disease (Payami *et al.*, 1997); females compared to males are at higher risk of both neurofibrillary tangle and amyloid-β plaque neuropathology especially in the early stages of Alzheimer's disease (Corder *et al.*, 2004; Damoiseaux *et al.*, 2012); greater education may allow people to harbour amyloid-β plaques and other brain pathology linked to Alzheimer's disease without experiencing decline in their cognitive functioning (Stern, 2012).

^{18}F-AV-1451 (also known as ^{18}F-T807) has been shown to bind selectively to paired-helical filament tau but not to other common protein aggregates such as amyloid-β, α-synuclein, and TDP-43 deposits in human brain tissues (Xia *et al.*, 2013; Marquie *et al.*, 2015). *In vivo* human studies indicate that patterns of ^{18}F-AV-1451 retention

parallel neuropathological staging of neurofibrillary tau pathology of Alzheimer's disease and that tracer retention increases with age even in the presence of cognitive impairment and dementia (Chien *et al.*, 2013; Johnson *et al.*, 2016; Scholl *et al.*, 2016). Florbetapir (also known as ^{18}F-AV-45 and Amyvid™) has been shown to bind to fibrillar forms of amyloid-β with high sensitivity and specificity in detection of presence and density of amyloid-β pathology with autopsy-verified histopathology (Choi *et al.*, 2009; Clark *et al.*, 2011). In this study, we specifically hypothesized that in a population of older people with various degrees of cognitive impairment: (i) ^{18}F-AV-1451 PET retention would be independently associated with age and cross-sectional florbetapir retention, and to a lesser degree with *APOE* genotype; and (ii) greater annualized change in amyloid-β burden in frontal, parietal, and lateral temporal brain regions, measured by longitudinal florbetapir PET scans antecedent to ^{18}F-AV-1451 PET scans, would be associated with greater ^{18}F-AV-1451 PET retention in limbic areas of inferior and lateral temporal and parietal lobes, i.e. brain sites of tau tangle deposition involved in early symptomatic disease stages. Furthermore, we hypothesized that the variance in cognitive performance and clinical outcome measures explained by this increased ^{18}F-AV-1451 retention pattern would be greater than, and independent of, the variance explained by the associated pattern of increased annualized change in florbetapir retention antecedent to ^{18}F-AV-1451 scan.

Materials and methods

Participants

Subjects of this study were ADNI-2 participants who recently underwent ^{18}F-AV-1451 PET imaging and had antecedent longitudinal florbetapir PET scans and structural MRI. ADNI is a longitudinal multi-centre natural history study designed to characterize clinical, imaging, genetic, and biochemical biomarkers for early detection and tracking of Alzheimer's disease (Weiner *et al.*, 2015). As of 12 September 2016, ^{18}F-AV-1451 PET imaging has been performed at 20 ADNI sites qualified for both ^{18}F-AV-1451 and florbetapir PET scanning. According to the clinical assessment done closest in time to ^{18}F-AV-1451 PET scan visit, the study cohort was composed of 42 clinically normal elderly individuals and 40 individuals with mild cognitive impairment (MCI). The diagnostic criteria for clinically normal and MCI in ADNI were previously described (Petersen *et al.*, 2010). In this study, we limited the longitudinal florbetapir PET scans to the last two time points (i.e. last visit closest to the time of the ^{18}F-AV-1451 PET scan and the one prior to the last).

PET acquisition

The radiochemical synthesis of both ^{18}F-AV-1451 and florbetapir were overseen and regulated by Avid Radiopharmaceuticals and distributed to the qualifying ADNI sites. PET imaging was performed at each ADNI site according to standardized protocols. The florbetapir protocol entailed the injection of 10 mCi of tracer followed by an uptake phase of 50 min. At 50 min subjects were positioned in the scanner and 4 × 5 min frames of emission data collected. This approach assisted with correction for patient movement as needed. Similarly, the ^{18}F-AV-1451 protocol entailed the injection of 10 mCi of tracer followed by an uptake phase of 80 min during which the subjects remained out of the scanner. ^{18}F-AV-1451 emission data were collected as 4 × 5 min frames from 80–100 min. PET/CT scans preceded these acquisitions with a CT scan for attenuation correction; PET-only scanners performed a transmission scan following the emission scan. Both PET scans underwent a rigorous quality control protocol and were processed to produce final images with standard orientation, voxel size, and 8 mm^3 resolution (Jagust *et al.*, 2010).

MRI acquisition

Structural MRIs were acquired at ADNI-2 sites equipped with 3 T MRI scanners using a 3D MP-RAGE or IR-SPGR T_1-weighted sequences with sagittal slices and voxel size of 1.1 × 1.1 × 1.2 mm^3, as described online (http://adni.loni.usc.edu/methods/documents/mri-protocols).

PET processing

Longitudinal florbetapir PET scans were analysed in native space using each participant's structural MRIs acquired closest to the time of the florbetapir PET scans. Briefly, structural MRIs were segmented into cortical regions of interest and reference regions in native space for each subject using FreeSurfer version 4.5.0 (surfer.nmr.mgh.harvard.edu/) as described previously (Landau *et al.*, 2012). Florbetapir data were realigned, and the mean of all frames was used to co-register florbetapir data to each participant's structural MRI. Cortical standardized uptake value ratio (SUVR) images for each subject at each time point were generated by dividing the voxel-wise florbetapir data by average uptake from a composite reference region (including the whole cerebellum, pons/brainstem, and eroded subcortical white matter regions) optimized for longitudinal florbetapir SUVR analysis (Landau *et al.*, 2015). The averaged cortical florbetapir SUVR in lateral and medial frontal, anterior and posterior cingulate, lateral parietal, and lateral temporal cortical grey matter regions was used as an index of global cortical florbetapir burden of each subject at each time point. Furthermore, subjects were characterized as florbetapir-positive (florbetapir+) or florbetapir-negative (florbetapir−) based on a threshold value of 0.79 as published previously (Landau *et al.*, 2015).

^{18}F-AV-1451 data were realigned, and the mean of all frames was used to coregister ^{18}F-AV-1451 data to each participant's MRI acquired closest to the time of the ^{18}F-AV-1451 PET. In each participant's MRI native space, we created ^{18}F-AV-1451 SUVR images based on mean ^{18}F-AV-1451 uptake normalized to uptake in a grey matter masked cerebellum reference region.

MRI processing

A designated centre quality controlled the MP-RAGE/IR-SPGR images and corrected for system-specific image artefacts such

as geometry distortion, B1 non-uniformity, and intensity inhomogeneities (Jack *et al.*, 2008). Further structural MRI processing was performed to established anatomical correspondences across subjects and time points to perform voxel-wise PET data analysis as described below. The structural MRI processing was based on the publicly available and open-source Advanced Normalization Tools (ANTs, http://stnava.github.io/ANTs/) and the associated pipelining framework PipeDream (http://neuropipedream.sourceforge.net). Briefly, corrected structural MRIs were mapped to an open source ageing brain template (IXI template) (Tustison *et al.*, 2014) via a symmetric diffeomorphic spatial normalization methodology available in ANTs (Avants *et al.*, 2008). The template contains prior labelling and probability maps that were used to aid both brain extraction and neuroanatomical segmentation. ^{18}F-AV-1451 and florbetapir SUVR images mapped onto template image space via the spatial normalization parameters estimated for the corresponding structural MRIs were used for subsequent data analyses.

Clinical and cognitive assessments

ADNI participants are assessed with a wide spectrum of clinical and cognitive tests (Aisen *et al.*, 2010). In this study, we limited the clinical assessments to the global Clinical Dementia Rating (CDR) based on CDR Sum of Boxes (CDR-SB) score and the Mini-Mental State Examination (MMSE) score based on a 30-point questionnaire, and limited the cognitive assessments to composite scores on two cognitive domains, memory and executive function (Crane *et al.*, 2012; Gibbons *et al.*, 2012). The composite score for memory was composed of scores of the Rey's Auditory Vocabulary List Test (RAVLT), Alzheimer's Disease Assessment Scale - cognitive subscale-11 (ADAS-Cog), Logical Memory (LM), and MMSE recall scores. The composite score for executive function included Category Fluency (animals and vegetables scores), Trail Making Test (TMT) A and B, Digit span backwards, Wechsler Adult Intelligence Scale-Revised (WAIS-R) Digit Symbol Substitution, and five Clock drawing items (circle, symbol, numbers, hands, time). Both composite scores were defined to have a mean of 0 and variance of 1 at the baseline visit, based on the 800 ADNI participants with complete cognitive assessments data.

Demographic and clinical features at the time of ^{18}F-AV-1451 scans

Differences in baseline characteristics between groups were assessed using analysis of variance with *post hoc* Bonferroni tests for continuous variables and χ^2 and Kruskal-Wallis with *post hoc* Mann-Whitney U-tests for dichotomous or categorical variables.

Relationships between ^{18}F-AV-1451 and Alzheimer's disease-related factors

Alzheimer's disease-related factors considered in this study included age at ^{18}F-AV-1451 PET scan visit, gender, education, *APOE* ε4 allele carrier status (0 or 1), and global cortical florbetapir burden measured closest to the ^{18}F-AV-1451 PET scan visit in time. We used a generalized linear model (GLM) for voxel-wise analysis of the ^{18}F-AV-1451 SUVR data as the dependent variable regressed against the explanatory variables age, gender, education, *APOE* ε4 allele status, and global cortical florbetapir burden closest to the ^{18}F-AV-1451 PET scan time across all subjects. The models presented herein were corrected for clinical diagnosis. Furthermore, models assessing the main effect of the global cortical florbetapir burden closest to the ^{18}F-AV-1451 PET scan time were further corrected for potential confounding effect of time between the last florbetapir-PET and ^{18}F-AV-1451 PET scans.

To assess the independent association of each Alzheimer's disease-related factor with ^{18}F-AV-1451 SUVR at voxel level after correcting for confounding effects of the remaining Alzheimer's disease-related factors, we compared pair-wise full GLM models with and without the Alzheimer's disease-related factor of interest, fitted by maximum likelihood (ML), via *F*-tests. These tests were performed separately for each Alzheimer's disease-related factor considered in this study. Due to substantial spatial correlations within imaging data, statistical significances were assessed after non-parametric correction for multiple-comparisons. Specifically, clusters of voxels exceeding a predetermined threshold ($P < 0.05$) were identified, and cluster-wise statistical significances were calculated via 1000 instances of a Monte Carlo simulation (Hayasaka *et al.*, 2006).

Relationships between ^{18}F-AV-1451 and antecedent annualized change in florbetapir

The relationship between ^{18}F-AV-1451 retention and antecedent annualized change in florbetapir retention was modelled using two different analysis approaches.

In the first analysis, we took a global influence approach and first estimated the linear change in the global cortical florbetapir burden based on the last two time point florbetapir-PET scans, then normalized by time difference between scans measured in years to estimate the annualized change in global cortical florbetapir burden. At each imaging voxel, we then used pair-wise GLMs across all subjects with voxel-wise ^{18}F-AV-1451 SUVR as the dependent variable with and without the annualized change in global cortical florbetapir burden as the explanatory variable while adjusting for age, gender, education, *APOE* ε4 allele status, global cortical florbetapir burden at the initial florbetapir-PET scan time, and the time from the last florbetapir-PET scan visit to the ^{18}F-AV-1451 PET scan visit. Pair-wise GLMs were then compared via *F*-tests and thresholded at cluster-wise statistical significances at $P < 0.05$ as estimated from 1000 instances of a Monte Carlo simulation (Hayasaka *et al.*, 2006).

In the second analysis, rather than performing univariate voxel-wise testing against the annualized change in global cortical florbetapir burden, we used a dimensionality reduction method based on sparse canonical correlation analysis specifically developed for medical imaging data (Le Cao *et al.*, 2009; Witten *et al.*, 2009; Avants *et al.*, 2010). Univariate approaches when applied at each imaging voxel lack statistical power due to severe multiple comparisons problem. Even if the statistical power could be boosted with greater sample sizes,

univariate methods do not exploit the latent signal in the image data that spreads across brain regions. We used the sparse canonical correlation analysis to extract the most dominant features associating ^{18}F-AV-1451 SUVR patterns and patterns of annualized change in florbetapir SUVR across all subjects, with the expectation of spatially disjointed multivariate associations. For this purpose, linear rates of florbetapir SUVR images were estimated as voxel-wise differences between last two time point florbetapir SUVR images, normalized by time difference between scans measured in years to estimate the annualized change in florbetapir retention voxel-wise. Permutation testing was performed to assess whether the associated multimodal PET patterns were significant while controlling for confounding effects of age, gender, education, *APOE* ε4 allele status, global cortical florbetapir burden at the initial florbetapir-PET scan time, and the time from the last florbetapir-PET scan visit to the ^{18}F-AV-1451 PET scan visit.

Previous studies reported that the dynamics of amyloid-β accumulation across brain regions were variable and associated with the global cortical amyloid-β burden (Villain *et al.*, 2012). Therefore, the analyses assessing the relationships between ^{18}F-AV-1451 and antecedent annualized change in florbetapir retention was repeated for florbetapir− and florbetapir+ sub-cohorts.

Variance in cognitive/clinical measures explained by ^{18}F-AV-1451 and antecedent annualized change in florbetapir

To leverage the dimensionality reduction via sparse canonical correlation analysis, projected values of ^{18}F-AV-1451 and annualized change in florbetapir retention for each subject were determined from the detected voxels within the associated multimodal PET patterns. The projected values were then used in subsequent data analysis to assess to what extent the annualized change in florbetair retention pattern and the associated ^{18}F-AV-1451 pattern explained the variance in global clinical and cognitive measures, both separately and jointly.

Results

Study cohort characteristics

Demographic and clinical characteristics are presented in Table 1. Diagnostic grouping was based on the most recent change in clinical diagnosis evaluation provided by the ADNI Clinical Core. The diagnostic groups did not differ in age at ^{18}F-AV-1451 PET visit, female/male gender distribution, *APOE* ε4 allele status distribution, and years of education. At the time of ^{18}F-AV-1451 PET visit, MCI subjects compared to clinically normal subjects were more impaired on both composite memory score ($P < 10^{-4}$) and composite executive function score ($P = 0.008$) and had greater CDR-SB ($P < 10^{-13}$) and marginally lower MMSE ($P = 0.03$) scores. The diagnostic groups did not differ in their florbetapir SUVR characteristics either at initial or last florbetapir-PET visits considered in this study. Furthermore, the groups did not differ in estimates of annualized change in global cortical florbetapir burden. There were no group differences in the time interval between the last florbetapir-PET and ^{18}F-AV-1451 PET scans.

We assessed partial correlation of clinical and cognitive measures with age, gender, education, *APOE* ε4 allele status, and global cortical florbetapir burden across all subjects while controlling for the remaining Alzheimer's disease-related factors. CDR-SB score was partially correlated with age ($r = 0.22$, $P < 10^{-4}$), gender ($r = 0.11$, $P = 0.04$), and global cortical florbetapir burden ($r = 0.12$, $P = 0.03$) but not education or *APOE* ε4 allele status. MMSE score was partially correlated with age ($r = -0.49$, $P < 10^{-20}$), gender ($r = -0.11$, $P = 0.04$), and global cortical florbetapir burden ($r = -0.26$, $P < 10^{-5}$) but not education or *APOE* ε4 allele status. Composite memory score was partially correlated with age ($r = -0.33$, $P < 10^{-8}$), gender ($r = -0.26$, $P < 10^{-5}$), education ($r = 0.15$, $P = 0.007$), *APOE* ε4 allele status ($r = -0.13$, $P = 0.02$), and global cortical florbetapir burden ($r = -0.14$, $P = 0.01$). Finally, composite executive function score was partially correlated only with age ($r = -0.16$, $P = 0.004$) and education ($r = 0.19$, $P = 0.0004$).

^{18}F-AV-1451 SUVR images of cognitively normal and early symptomatic subjects

Figure 1 shows average patterns of ^{18}F-AV-1451 PET SUVR images of florbetapir− and florbetapir+ participants from each diagnostic group. Although voxel-wise contrasts between groups were not assessed in this study, the *in vivo* ^{18}F-AV-1451 SUVR patterns were visually consistent with the patterns observed in previous post-mortem and *in vivo* ^{18}F-AV-1451 PET studies (Braak and Braak, 1997*a*; Johnson *et al.*, 2016; Scholl *et al.*, 2016). Specifically, the florbetapir− clinically normal subjects had low overall cortical ^{18}F-AV-1451 binding with presumably off-target ^{18}F-AV-1451 binding at basal ganglia, whereas more extensive medial temporal lobe binding was observed in the florbetapir+ clinically normal subjects. Greater medial temporal lobe ^{18}F-AV-1451 binding with more extensive neocortical binding, especially in parietal and temporal regions, and selective sparing of primary cortices was observed with increased symptomatology as in MCI subjects. Similar to clinically normal subjects, the extent and magnitude of the ^{18}F-AV-1451 binding were amplified with florbetapir-positivity in MCI subjects.

^{18}F-AV-1451 binding in relation to Alzheimer's disease-related factors

In voxel-wise statistical analyses across all subjects assessing the associations between ^{18}F-AV1451 SUVR and each of the Alzheimer's disease-related factors without correcting

Table 1 Study cohort characteristics

	CN	MCI	*P*
n	42	40	n.s.
Age (years)	74.87 ± 6.98	77.21 ± 7.13	n.s.
Gender (F/M)	22/20	14/26	n.s.
APOE4 (−/+)	24/18	29/11	n.s.
Education (years)	16.19 ± 2.48	16.88 ± 2.64	n.s.
CDR at AV-145 scan	0.04 ± 0.13	0.39 ± 0.21	$< 10^{-13}$
MMSE at AV-1451 scan	28.90 ± 1.20	28.10 ± 2.01	0.03
Composite memory at AV-1451 scan	1.23 ± 0.69	0.54 ± 0.75	$< 10^{-4}$
Composite executive function at AV-1451 scan	0.98 ± 0.67	0.54 ± 0.82	0.008
Initial florbetapir-PET scan	41	37	
Global cortical florbetapir burden	0.80 ± 0.11	0.82 ± 0.12	n.s.
Florbetapir −/+	26/15	20/17	n.s.
Last florbetapir-PET scan	41	37	
Global cortical florbetapir burden	0.81 ± 0.12	0.84 ± 0.13	n.s.
Florbetapir −/+	25/16	16/21	n.s.
Time from initial florbetapir-PET scan (years)	2.11 ± 0.36	2.08 ± 0.34	n.s.
Time to AV-1451-PET scan (years)	0.72 ± 0.83	0.84 ± 0.91	n.s.
Annualized change in global cortical florbetapir burden	0.0060 ± 0.0119	0.0047 ± 0.0120	n.s.

n.s. = non-significant; CN = cognitively normal.

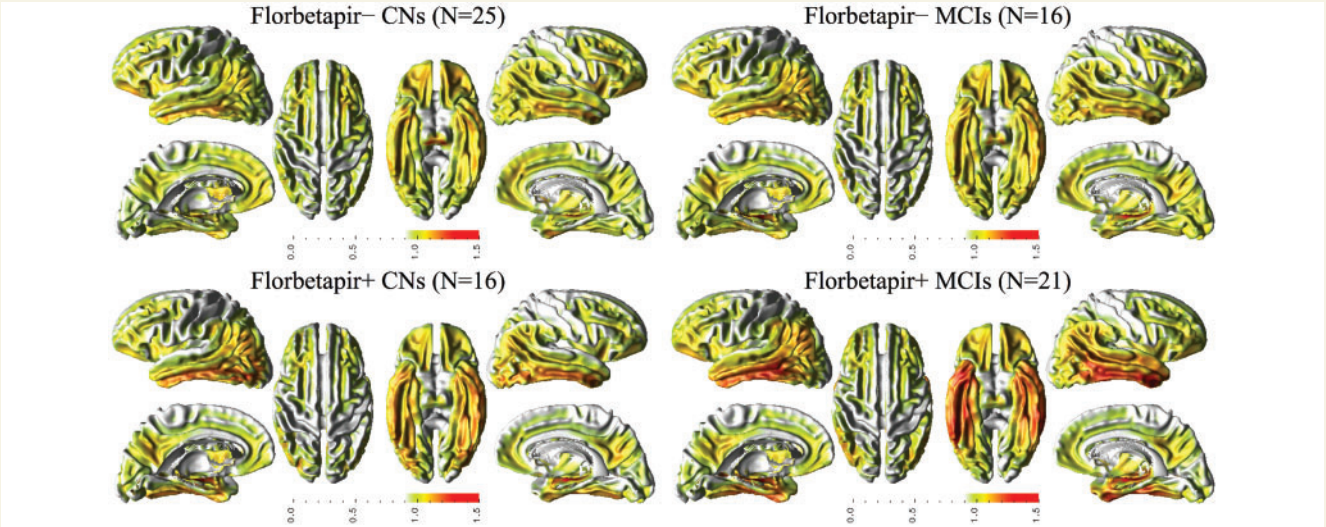

Figure 1 Average patterns of ^{18}F-AV-1451 PET SUVR (cerebellar grey matter reference) images of florbetapir− and florbetapir+ participants from each diagnostic group.

for confounding effects of the remaining Alzheimer's disease-related factors, we found that (i) cortical ^{18}F-AV-1451 binding was positively associated with age in temporal pole and medial orbitofrontal regions, with *APOE* ε4 allele carrier status in hippocampus, and with global cortical florbetapir burden throughout medial and lateral temporal, lateral occipital and inferior parietal regions; (ii) cortical ^{18}F-AV-1451 binding was negatively associated with age, particularly in medial frontal brain regions, with male gender in lateral parieto-temporal regions, and with education in lateral occipital region; and (iii) presumably off-target subcortical ^{18}F-AV-1451 binding was positively associated with age and male gender (Supplementary Fig. 1).

The independent relationships between these Alzheimer's disease-related factors and ^{18}F-AV-1451 binding were as follows: (i) controlling for gender, education, *APOE* ε4 allele carrier status, global cortical florbetapir burden, and the time interval between the last florbetapir-PET and ^{18}F-AV-1451 PET scans, advanced age across all subjects was associated with greater presumably off-target ^{18}F-AV-1451 binding in basal ganglia and greater temporal pole and medial orbitofrontal ^{18}F-AV-1451 binding, but lower ^{18}F-AV-1451 binding in anterior aspects of medial frontal cortices (Fig. 2A). As global cortical florbetapir burden positively correlates with age ($r = 0.16$, $P = 0.004$), to test if correcting for confounding effects of global cortical

florbetapir burden artificially introduced negative associations between age and ^{18}F-AV-1451 binding, analysis was repeated only controlling for gender, education, and *APOE* ε4 allele carrier status. Although negative association findings between age and ^{18}F-AV-1451 binding did not change, additional significant positive associations between age and ^{18}F-AV-1451 binding were observed in hippocampus and amygdala regions (Fig. 2B); (ii) increased global cortical florbetapir burden was associated with greater ^{18}F-AV-1451 binding in diffuse cortical regions, including inferior and middle temporal regions, medial and inferior parietal cortices, and prefrontal regions (Fig. 2C), after correcting for age, gender, education, *APOE* ε4 allele carrier status, and the time interval between the last florbetapir-PET and ^{18}F-AV-1451 PET scans. Gender, education, and *APOE* ε4 allele carrier status effects on ^{18}F-AV-1451 binding were not significant after controlling for confounding effects of the remaining Alzheimer's disease-related factors considered in this study (data not shown).

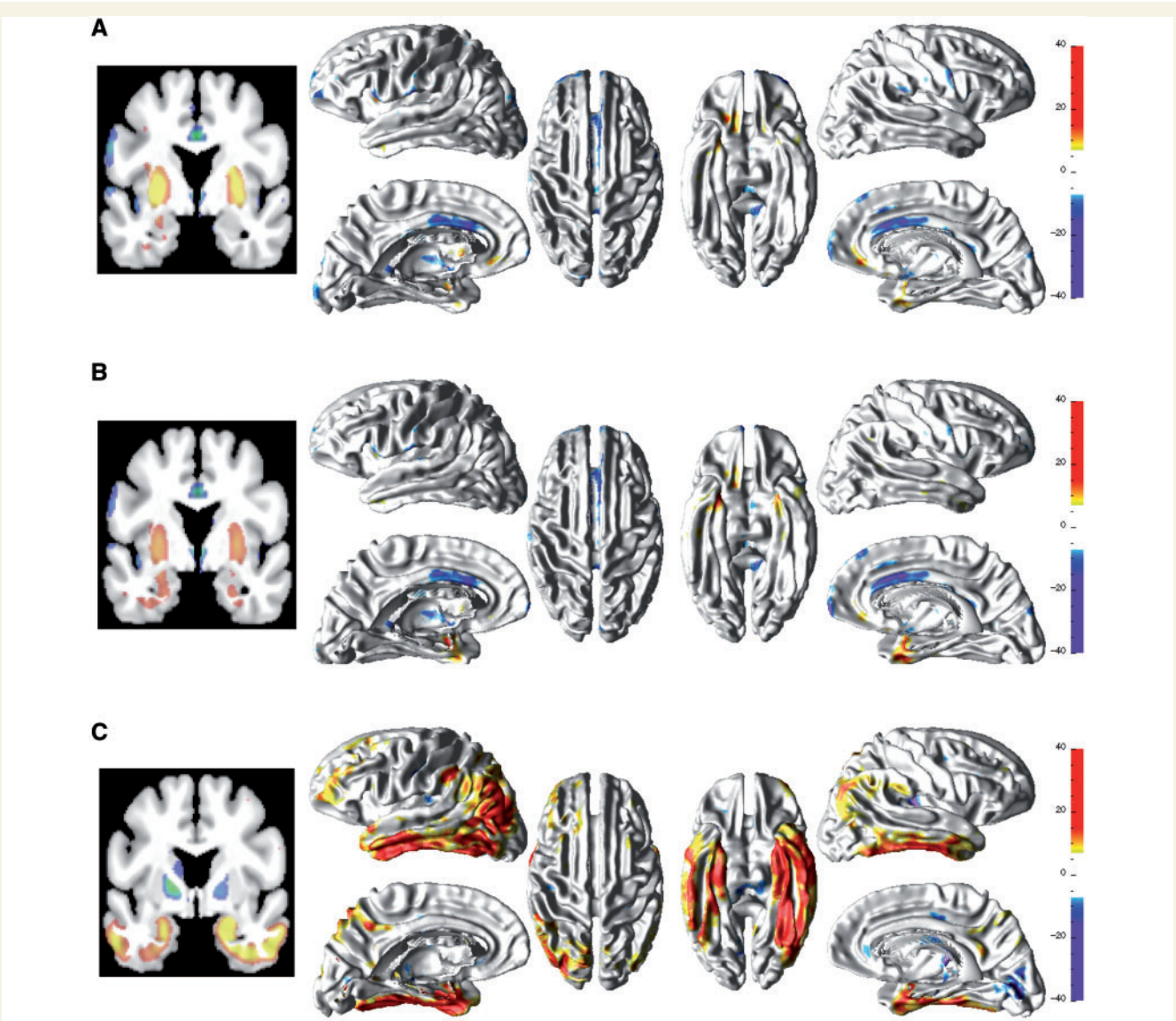

Figure 2 Relationships between ^{18}F-AV1451 SUVR and Alzheimer's disease-related factors. (**A**) Age and ^{18}F-AV-1451 SUVR association corrected for gender, education, *APOE* ε4 allele status, and global cortical florbetapir burden. (**B**) Age and ^{18}F-AV-1451 SUVR association corrected for gender, education, *APOE* ε4 allele status, but not global cortical florbetapir burden. (**C**) Global cortical florbetapir burden and ^{18}F-AV-1451 SUVR association corrected for age, gender, education, *APOE* ε4 allele status, and the time from the last florbetapir-PET to the ^{18}F-AV-1451 scan. Covariate adjusted significance maps ($P < 0.05$; cluster-level corrected). Hot colours: positive associations; cold colours: negative associations.

^{18}F-AV-1451 binding in relation to annualized change in global florbetapir burden antecedent to ^{18}F-AV1451 PET scans

On average, clinically normal subjects had the greater annualized change in global cortical florbetapir burden, compared to MCI subjects, without statistical significance at group level (Table 1). Subjects identified as florbetapir + at the initial florbetapir-PET scan had marginally greater ($P = 0.06$) annualized change in global cortical florbetapir burden compared to the change observed in subjects identified as florbetapir− at the initial florbetapir-PET scan visit.

We observed no significant association between voxel-wise ^{18}F-AV-1451 binding and antecedent annualized change in global cortical florbetapir burden using a univariate regression model across all subjects, florbetapir− subjects only, or florbetapir + subjects only (data not shown).

^{18}F-AV-1451 binding in relation to voxel-wised annualized change in florbetapir binding antecedent to ^{18}F-AV1451 PET scans

Average maps of annualize change in florbetapir SUVR within florbetapir− ($n = 41$) and florbetapir + ($n = 37$) subjects are shown in Supplementary Fig. 2. Florbetapir−/+ dichotomization was based on the initial florbetapir-PET scan analysis. On average, we observed increase in florbetapir SUVR throughout the cortex, with the greatest changes in the lateral temporal, medial inferior temporal, inferior parietal, medial parietal, inferior frontal, and medial orbitofrontal cortices. Although florbetapir + subjects, compared to florbetapir− subjects, had greater annualized change in florbetapir SUVR throughout the brain, florbetapir− versus florbetapir + group differences were not significant in voxel-wise statistical analysis.

We used sparse canonical correlation analysis to assess the extent to which increased annualized change in florbetapir binding and spatial patterns of ^{18}F-AV-1451 binding were associated in our cohort. This was achieved by computing a reduced, optimal weighted average of a set of voxels in each modality that maximizes the correlation between multimodal measures. In the context of this study, sparse canonical correlation analysis aimed to isolate networks of voxels, potentially distinct for each modality, such that they collectively relate to each other with the highest correlation possibly attained within this cohort. This sparse selection of network of voxels was spatially distributed and automatically identified by using a regularized energy minimization approach to define the sets of voxels in one modality that were most informative about the other and the most reliable.

Sparse canonical correlation analysis solution vectors (i.e. weight vectors) are shown in Fig. 3, where the brightness of the red-hued overlay is related to the solution's weighting at the local voxel. Sparse canonical correlation analysis indicated a pattern of increased annualized change in florbetapir binding in predominantly right lateral temporal and supramarginal regions, and bilateral precuneus/posterior cingulate cortices that was significantly associated with a pattern of greater ^{18}F-AV-1451 binding in hippocampus, fusiform gyrus, inferior temporal, and inferior parietal lobule predominantly in the left hemisphere ($r = 0.27$; $P < 10^{-7}$). When repeated within florbetapir− subjects only, sparse canonical correlation analysis indicated a pattern of increased annualized change in florbetapir binding in the superior frontal and anterior cingulate cortices bilaterally that was significantly associated with a pattern of greater ^{18}F-AV-1451 binding in the hippocampus, fusiform gyrus, inferior temporal, and inferior parietal lobule as well as the superior frontal cortex bilaterally, as shown in Fig. 4 ($r = 0.54$; $P < 10^{-15}$). When repeated within florbetapir + subjects only, sparse canonical correlation analysis identified two associated pattern pairs: the first associated pattern pair mirrored the pattern of increased annualized change in florbetapir binding and associated greater ^{18}F-AV-1451 binding pattern seen in the full cohort sparse canonical correlation analysis, as shown in Fig. 5A and B ($r = 0.39$; $P < 10^{-6}$). The second associated pattern pair shown in Fig. 5C and D indicated a pattern of increased annualized change in florbetapir binding in the bilateral middle frontal, right pars opercularis, right lateral inferior temporal, left angular gyrus and superior temporal, and bilateral lingual gyrus regions that was significantly associated with a pattern of greater ^{18}F-AV-1451 binding in the left precuneus/posterior cingulate, bilateral medial and lateral orbitofrontal cortices, and right inferior parietal lobule ($r = 0.20$; $P < 0.01$).

Relationship between brain tau (^{18}F-AV-1451), brain amyloid-β (florbetapir) and cognitive/clinical measures

In full cohort assessment, the pattern of greater ^{18}F-AV-1451 binding identified by the sparse canonical correlation analysis explained 24% of the variance in the composite memory score ($P = 0.0004$), but none of the variance in the CDR-SB, MMSE, or composite executive function scores. Although the pattern of increased annualized change in florbetapir binding did not explain variance in any cognitive/clinical measures independently, jointly with the pattern of greater ^{18}F-AV-1451 binding explained 23% of the variance in the MMSE ($P = 0.0008$).

In the florbetapir− only subcohort, the pattern of greater ^{18}F-AV-1451 binding identified by the sparse canonical correlation analysis explained 48% of the variance in MMSE score ($P < 10^{-4}$) and 23% of the variance in composite memory score ($P = 0.02$). The pattern of increased

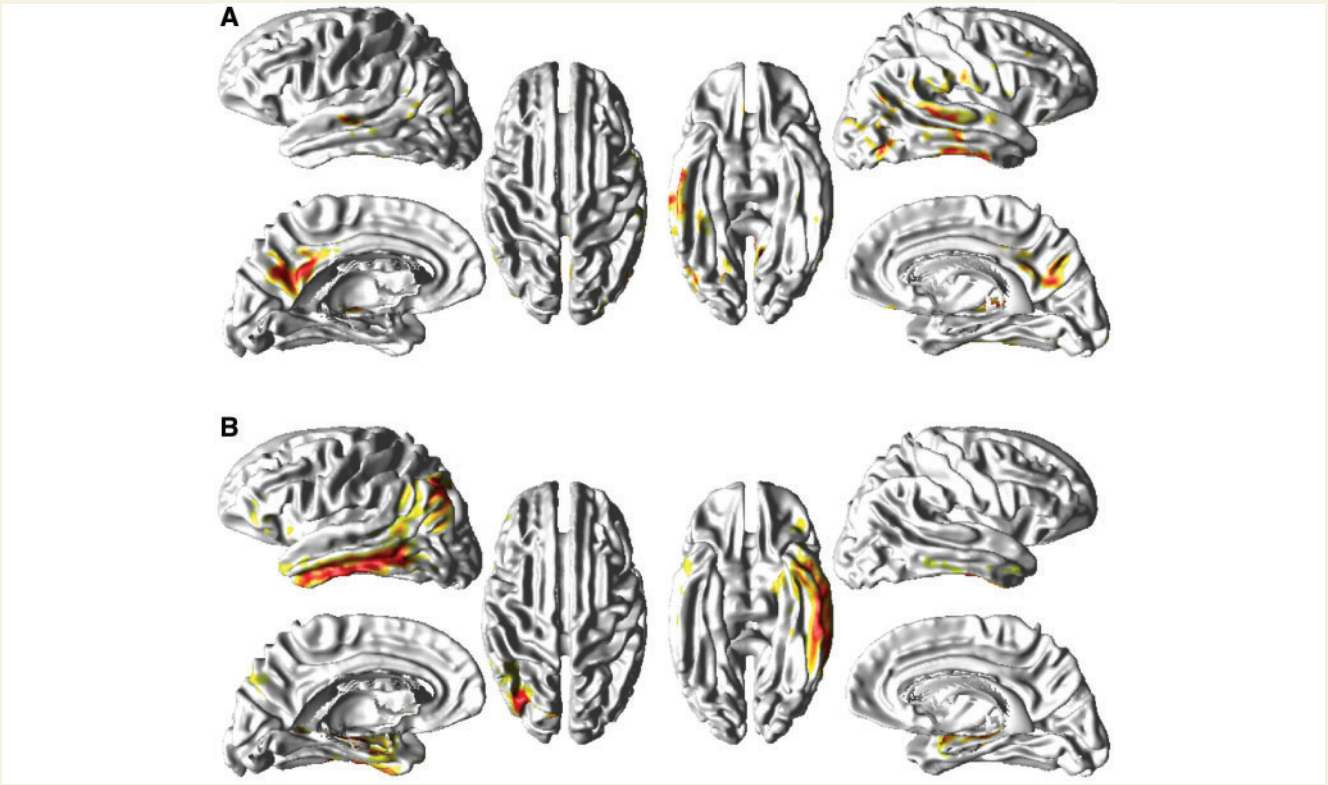

Figure 3 Relationship between ^{18}F-AV1451 SUVR and antecedent annualized change in florbetapir-SUVR identified using sparse canonical correlation analysis of all subjects ($r = 0.27$, $P < 10^{-7}$). (**A**) Pattern of annualized change in florbeatpir antecedent to ^{18}F-AV-1451-PET scan. (**B**) Pattern of greater ^{18}F-AV-1451 binding associated with greater annualized change in florbetapir pattern in **A**.

annualized change in florbetapir binding explained 34% of the variance in MMSE score ($P = 0.002$) but did not add value to the pattern of greater ^{18}F-AV-1451 binding in explaining variance in MMSE score.

In the florbetapir+ only sub-cohort, neither the first pattern of greater ^{18}F-AV-1451 binding nor the first pattern of increased annualized change in florbetapir binding explained variance in any cognitive/clinical measure independently. The second pattern of greater ^{18}F-AV-1451 binding explained 32% of the variance in the composite memory score ($P = 0.02$).

As exploratory analyses, we tested the main effect of global florbetapir burden and the main effects of voxel-wise florbetapir SUVR measures on clinical/cognitive measures considered in this study, cross-sectional. None of the analyses reached statistical significance.

Discussion

In this study, we assessed the patterns of ^{18}F-AV-1451 binding associated with well-established Alzheimer's disease factors and global clinical and cognitive outcome measures in a cohort including cognitively healthy elderly individuals and individuals at early symptomatic stages of Alzheimer's disease. Furthermore, we explored highly associated patterns of greater ^{18}F-AV-1451 binding and increased annualized change in florbetapir binding antecedent to ^{18}F-AV-1451 PET, and to what extent this multimodal pattern association explained the variance in cognitive performance and clinical outcome measures, independently and jointly. One major difference between this work and all previously reported studies using tau PET ligands is that, in addition to classical voxel-based analysis, we used multivariate neuroimaging statistics respecting the spatial disconnect between amyloid-β and tau pathologies.

Our major findings were as follows: (i) ^{18}F-AV-1451 PET retention was differentially associated with age and cross-sectional florbetapir PET retention; (ii) increased annualized change in florbetapir retention, antecedent to ^{18}F-AV-1451 PET scans, prominently in the parieto-temporal brain regions as well as superior and medial frontal brain regions, was associated with greater ^{18}F-AV-1451 PET retention most prominently in the inferior temporal, lateral parietal, and to a lesser degree in the precuneus/posterior cingulate and orbitofrontal brain regions in the full cohort, with florbetapir−/+ associated variability; and (iii) greater ^{18}F-AV-1451 PET retention associated with increased annualized change in florbetapir retention, antecedent to ^{18}F-AV-1451 PET scans, significantly explained variance in global clinical outcome measures, and this was independent of the increased annualized change in florbetapir retention.

The first major finding was that ^{18}F-AV-1451 PET retention was independently associated with age and cross-

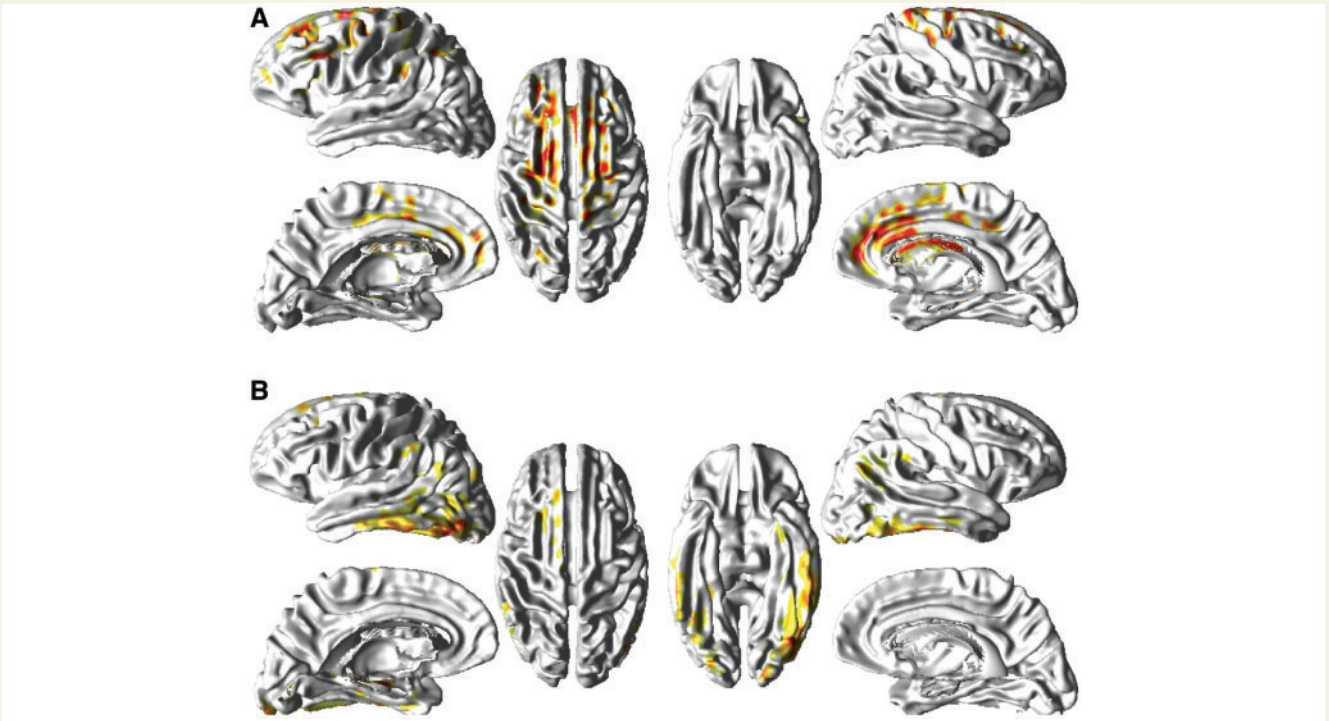

Figure 4 Relationship between ^{18}F-AV1451 SUVR and antecedent annualized change in florbetapir-SUVR identified using sparse canonical correlation analysis of florbetapir− subjects ($r = 0.54$, $P < 10^{-15}$). (**A**) Pattern of annualized change in florbeatpir antecedent to ^{18}F-AV-1451-PET scan. (**B**) Pattern of greater ^{18}F-AV-1451 binding associated with greater annualized change in florbetapir pattern in **A**.

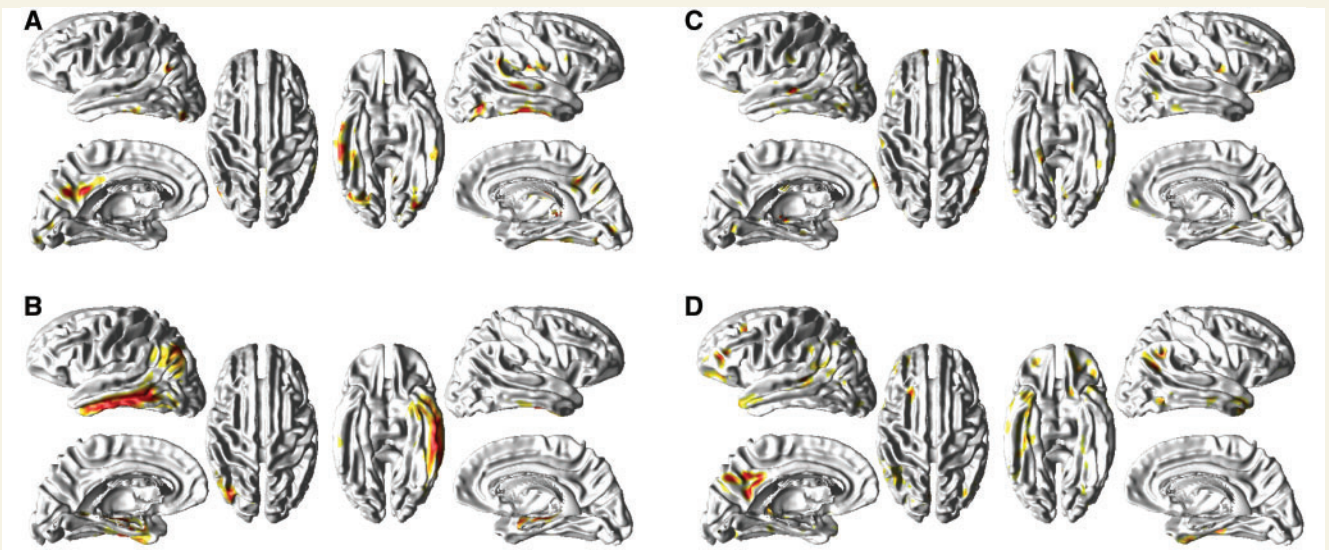

Figure 5 Relationship between ^{18}F-AV1451 SUVR and antecedent annualized change in florbetapir-SUVR identified using sparse canonical correlation analysis of florbetapir+ subjects ($r = 0.54$, $P < 10^{-15}$). (**A**) First pattern of annualized change in florbetapir antecedent to ^{18}F-AV-1451-PET scan. (**B**) First pattern of greater ^{18}F-AV-1451 binding associated with greater annualized change in florbetapir pattern in **A**. (**C**) Second pattern of annualized change in florbetapir antecedent to ^{18}F-AV-1451-PET scan. (**D**) Second pattern of greater ^{18}F-AV-1451 binding associated with greater annualized change in florbetapir pattern in **C**.

sectional florbetapir PET retention, but not with education, gender, or *APOE* ε4 genotype. This main observation was in line with neuropathology literature consistently reporting significant influence of age and amyloid-β on formation of neurofibrillary tau tangles but a lack of independent effect of *APOE* ε4 genotype on neurofibrillary tau tangle formation (Serrano-Pozo *et al.*, 2015; Mufson *et al.*, 2016). Although the literature on association between *in vivo* ^{18}F-AV-1451 PET retention and the Alzheimer's disease-related factors is very limited at this point, our interpretation of these findings is as follows: (i) After correcting for global cortical florbetapir burden, advanced age was associated with greater ^{18}F-AV-1451 retention in the basal forebrain, temporal pole, and to some extent in the medial temporal lobe. Weaker age-associated ^{18}F-AV-1451 retention findings especially in the hippocampus and entorhinal cortex might be due to off-target binding in adjacent structures (Marquie *et al.*, 2015) and relatively greater partial volume effects induced by greater tau-associated atrophy in these structures. Consistent with our findings, one *in vivo* ^{18}F-AV-1451 PET study previously reported advanced age associated greater *in vivo* ^{18}F-AV-1451 PET retention in medial temporal lobe, basal forebrain, and insula in cognitively normal participants (Scholl *et al.*, 2016), while another notable study reported significant negative association between age and inferior temporal ^{18}F-AV-1451 PET retention in cognitively normal participants (Johnson *et al.*, 2016), both studies potentially capturing different aspects of age-related tau accumulation reported in large autopsy studies (Braak *et al.*, 2011). The strongest association between advanced age and greater ^{18}F-AV-1451 retention was observed in the basal ganglia. ^{18}F-AV-1451 retention in this region is largely considered off-target binding of the ^{18}F-AV-1451 tracer (Marquie *et al.*, 2015) since limited neurofibrillary pathology has been reported in the basal ganglia. Further ^{18}F-AV-1451 tracer validation studies are required to assess the biological substrates of the advanced age associated greater off-target binding of the tracer in the basal ganglia structures. In our cohort, after controlling for other Alzheimer's disease-related factors, advanced age was associated with lower ^{18}F-AV-1451 binding in the anterior aspects of the medial frontal cortical regions. First, we should emphasize that the current study is based on a convenience cohort where the degree of true population representation is not known. Second, most neuropathological changes associated with Alzheimer's disease are strongly associated with rapid disease progression only in younger elderly individuals (Savva *et al.*, 2009). Older age at disease onset was associated with lower tau and amyloid-β pathology (Silbert *et al.*, 2012). Given the high prevalence of florbetapir-positivity in our cohort, one explanation for this negative age-association in cortical ^{18}F-AV-1451 binding could be that individuals who had amyloid-β pathology early had a more rapid rise in brain amyloid-β leading to rapid accumulation of tau tangles. Another possible explanation is that for any given level of cognitive impairment, a younger person is more likely to have only Alzheimer's disease as the brain pathology. On the other hand, an older person is more like to have other pathologies than just Alzheimer's disease (i.e. tau pathology), such as—but not limited to—small strokes and white matter disease. (ii) We observed that female gender was associated with greater ^{18}F-AV-1451 binding in diffuse cortical regions including lateral temporal, parietal, and frontal regions, in analysis uncorrected for confounding effects. Both neuropathology and *in vivo* studies agree that males and females may differ in the pathologic substrate for Alzheimer's disease (Lin and Doraiswamy, 2014). Neuropathology studies suggest that females have a 3-year acceleration in tau tangle neuropathology (Corder *et al.*, 2004) and this gender difference was largely attributable to *APOE* ε4 carrier females. Future research is warranted to assess the gender and *APOE* ε4 genotype interaction on *in vivo* ^{18}F-AV-1451 binding. (iii) We observed lower ^{18}F-AV-1451 binding prominently in lateral occipital cortices being associated with higher levels of education, in analysis uncorrected for confounding effects. Epidemiological studies suggest that education, in addition to other lifelong experiences, is associated with lower prevalence of Alzheimer's disease (Sharp and Gatz, 2011; Lo and Jagust, 2013). Furthermore, previous data suggest that lifetime cognitive activity is associated with lower amyloid-β deposition (Vemuri *et al.*, 2011; Lo and Jagust, 2013). One explanation of this result is that education increases cognitive reserve (Stern, 2012). This may represent an intrinsic cortical mechanism for responding to the effects of pathology, in particular amyloid-β facilitated tau accumulation. (iv) Greater global amyloid-β burden measured by florbetapir PET retention was associated with greater ^{18}F-AV-1451 binding in diffuse cortical regions including inferior and middle temporal regions, medial and inferior parietal cortices, and prefrontal regions, consistent with large autopsy studies and recent *in vivo* ^{18}F-AV-1451 studies (Johnson *et al.*, 2016; Scholl *et al.*, 2016) as well as the idea that neocortical tau accumulation is associated with the high amyloid-β burden.

The second major finding was that antecedent increased annualized change in amyloid-β burden in frontal, parietal, and lateral temporal brain regions, measured by longitudinal florbetapir PET, was associated with greater ^{18}F-AV-1451 PET retention in limbic areas of medial and inferior temporal and parietal lobes, sites of tau tangle deposition involved in early symptomatic disease stages. A florbetapir−/+ associated variability was observed in this relationship between ^{18}F-AV1451 SUVR and antecedent annualized change in florbetapir-SUVR identified using sparse canonical correlation analysis. In particular, the multimodality pattern association in florbetapir− subjects was dominated by the annualized change in frontal florbetapir-SUVR with a relatively weaker increase in the inferior temporal and inferior parietal ^{18}F-AV1451 SUVR. Previous studies suggest that precuneus is the earliest cortical region to accumulate amyloid-β, closely followed by the cingulate and frontal cortices, then by the lateral parietal and temporal cortices (Bilgel *et al.*, 2016). This multimodality

pattern association in florbetapir− subjects might reflect the earliest tau deposition in the limbic areas due to the earliest amyloid-β spread. In addition, greater orbitofrontal ^{18}F-AV-1451 PET retention associated with increased annualized change in florbetapir retention was only observed in florbetapir+ subjects. According to Braak and Braak staging, increased anterior frontal tau pathology is seen in stages III-IV with increasing cognitive impairment (Braak *et al.*, 2011). Thus, this multimodal pattern association specific to florbetapir+ subjects may reflect a more advanced disease progression stage in florbetapir+ subjects. These findings are in general consistent with three important concepts in Alzheimer's disease research not yet fully validated with *in vivo* data. First, autopsy studies consistently associated the spread of tau outside the medial temporal lobe with increased amyloid-β pathology (Braak *et al.*, 1999). Second, the most prevailing Alzheimer's disease biomarker model suggests that amyloid-β aggregation facilitates the disease pathological cascade including the tau accumulation outside the medial temporal lobe (Jack *et al.*, 2013). Finally, transneuronal transmission on disease-specific networks drives divergent spatiotemporal progression of amyloid-β and tau (Raj *et al.*, 2012, 2015).

A long-term goal of our field is to determine the sequence of pathological events, which ultimately lead to cognitive decline and dementia. The ability to measure brain amyloid-β, tau, atrophy and cognition in a large group of subjects longitudinally will ultimately provide data, which will allow testing of the hypothesis that accumulation of brain amyloid-β leads to tau accumulation, which causes neurodegeneration measured by brain atrophy and cognitive decline. Our current ADNI dataset only has single time point ^{18}F-AV-1451 PET data, preventing a longitudinal analysis. However, we examined the feasibility of this approach using one time point by analysing the relationship of change in brain amyloid-β to brain tau to cognition. Thus our third major finding was that those brain regions that had tau tangles (measured by ^{18}F-AV-1451 PET retention) associated with increased annualized change in brain amyloid-β burden (measured by longitudinal florbetapir PET retention antecedent to the ^{18}F-AV-1451 PET scans), significantly explained the variance in cognitive performance and clinical outcome measures, and this was independent of the increased annualized change in florbetapir PET retention. In a region of interest analysis (Johnson *et al.*, 2016), greater inferior temporal ^{18}F-AV-1451 retention was related to greater impairment on MMSE and CDR-SB, with similar but weaker associations observed between greater global amyloid-β burden and greater impairment on MMSE and CDR-SB. In our data-driven multimodality analysis, we also observed that greater inferior temporal ^{18}F-AV-1451 retention, associated with increased annualized change in florbetapir retention in lateral temporal, lateral parietal, and orbitofrontal cortices, was significantly associated with global clinical outcome measures. Furthermore, it was not the increased annualized change in global amyloid-β burden, but increased annualized change in focal amyloid-β accumulation that greatly influenced the spread and severity of distant tau accumulation as detected by multimodal PET scans. These findings are in agreement with the pathology literature, which suggests that tau tangles but not amyloid-β plaques correlate with cognition (Markesbery, 1997), especially memory function (Terry *et al.*, 1999). Furthermore, cortical tau tangles are also associated with neurodegeneration (Braak and Braak, 1996; Bradley *et al.*, 2002; Ballatore *et al.*, 2007; Vemuri *et al.*, 2008), and are likely to be part of the chain of events leading to cortical dysfunction and cognitive impairment. Pathological studies (Braak and Braak, 1997*b*; Braak *et al.*, 2011) showed that during the early development of Alzheimer's disease pathology, tau tangles increase in the medial temporal lobe, associated with synapse loss and neurodegeneration, while at the same time widespread neocortical amyloid-β plaques are developing. According to the amyloid-β hypothesis (Hardy and Selkoe, 2002; Karran *et al.*, 2011), the accumulation of amyloid-β leads to downstream events including accumulation of tau tangles, neurodegeneration, cognitive decline and dementia.

A main strength of the present study is the inclusion of a variety of diagnostic groups including cognitively normal and early symptomatic subjects from a multi-centre study, which allowed us to study relationships between tau pathology and Alzheimer's disease-related factors in a continuum. At the same time, treating the cohort as a continuum in Alzheimer's disease pathophysiology could be a flaw in our study design. In particular, even with the evidence of Alzheimer's disease pathology, many of the clinically normal subjects and some of the MCI subjects will never develop Alzheimer's disease. As the subjects in our cohort are potentially samples from different populations (i.e. not necessarily on Alzheimer's disease path), the composition of the study cohort may be driving the associations observed in this study. Furthermore, MCI subjects are notoriously a very heterogeneous group and other pathologies, unrelated to Alzheimer's disease, may have contributed to variations in both tau and rates of amyloid-β. We should also note that this is a preliminary study with a relatively small sample size. Due to sample size limitations, we did not assess relationships between ^{18}F-AV-1451 PET, Alzheimer's disease-related factors, and brain atrophy. Future studies including more participants are needed to extend and replicate our findings.

Acknowledgements

Data used in preparation of this article were obtained from the Alzheimer's Disease Neuroimaging Initiative (ADNI) database (adni.loni.usc.edu). As such, the investigators within the ADNI contributed to the design and implementation of ADNI and/or provided data but did not participate in analysis or writing of this report. A complete listing of ADNI investigators can be found at: http://adni.loni.usc.edu/wp-content/uploads/how_to_apply/ADNI_Acknowledgement_List.pdf

Funding

Support for this study was provided by NIH U01-AG024904. Data collection and sharing for this project was funded by the Alzheimer's Disease Neuroimaging Initiative (ADNI) (National Institutes of Health Grant U01 AG024904). ADNI is funded by the National Institute on Aging, the National Institute of Biomedical Imaging and Bioengineering, and through generous contributions from the following: AbbVie, Alzheimer's Association; Alzheimer's Drug Discovery Foundation; Araclon Biotech; BioClinica, Inc.; Biogen; Bristol-Myers Squibb Company; CereSpir, Inc.; Eisai Inc.; Elan Pharmaceuticals, Inc.; Eli Lilly and Company; EuroImmun; F. Hoffmann-La Roche Ltd and its affiliated company Genentech, Inc.; Fujirebio; GE Healthcare; IXICO Ltd.; Janssen Alzheimer Immunotherapy Research & Development, LLC.; Johnson & Johnson Pharmaceutical Research & Development LLC.; Lumosity; Lundbeck; Merck & Co., Inc.; Meso Scale Diagnostics, LLC.; NeuroRx Research; Neurotrack Technologies; Novartis Pharmaceuticals Corporation; Pfizer Inc.; Piramal Imaging; Servier; Takeda Pharmaceutical Company; and Transition Therapeutics. The Canadian Institutes of Health Research is providing funds to support ADNI clinical sites in Canada. Private sector contributions are facilitated by the Foundation for the National Institutes of Health (www.fnih.org). The grantee organization is the Northern California Institute for Research and Education, and the study is coordinated by the Alzheimer's Disease Cooperative Study at the University of California, San Diego. ADNI data are disseminated by the Laboratory for Neuro Imaging at the University of Southern California.

Supplementary material

Supplementary material is available at *Brain* online.

References

Aisen PS, Petersen RC, Donohue MC, Gamst A, Raman R, Thomas RG, et al. Clinical core of the Alzheimer's disease neuroimaging initiative: progress and plans. Alzheimers Dement 2010; 6: 239–46.

Avants BB, Cook PA, Ungar L, Gee JC, Grossman M. Dementia induces correlated reductions in white matter integrity and cortical thickness: a multivariate neuroimaging study with sparse canonical correlation analysis. Neuroimage 2010; 50: 1004–16.

Avants BB, Epstein CL, Grossman M, Gee JC. Symmetric diffeomorphic image registration with cross-correlation: evaluating automated labeling of elderly and neurodegenerative brain. Med Image Anal 2008; 12: 26–41.

Ballatore C, Lee VM, Trojanowski JQ. Tau-mediated neurodegeneration in Alzheimer's disease and related disorders. Nat Rev Neurosci 2007; 8: 663–72.

Berg L, McKeel DW Jr, Miller JP, Storandt M, Rubin EH, Morris JC, et al. Clinicopathologic studies in cognitively healthy aging and Alzheimer's disease: relation of histologic markers to dementia severity, age, sex, and apolipoprotein E genotype. Arch Neurol 1998; 55: 326–35.

Bilgel M, Prince JL, Wong DF, Resnick SM, Jedynak BM. A multivariate nonlinear mixed effects model for longitudinal image analysis: application to amyloid imaging. Neuroimage 2016; 134: 658–70.

Braak E, Griffing K, Arai K, Bohl J, Bratzke H, Braak H. Neuropathology of Alzheimer's disease: what is new since A. Alzheimer? Eur Arch Psychiatry Clin Neurosci 1999; 249 (Suppl 3): 14–22.

Braak H, Braak E. Development of Alzheimer-related neurofibrillary changes in the neocortex inversely recapitulates cortical myelogenesis. Acta Neuropathologica 1996; 92: 197–201.

Braak H, Braak E. Frequency of stages of Alzheimer-related lesions in different age categories. Neurobiol Aging 1997a; 18: 351–7.

Braak H, Braak E. Staging of Alzheimer-related cortical destruction. Int Psychogeriatr 1997b; 9 (Suppl 1): 257–61; discussion 69–72.

Braak H, Thal DR, Ghebremedhin E, Del Tredici K. Stages of the pathologic process in Alzheimer disease: age categories from 1 to 100 years. J Neuropathol Exp Neurol 2011; 70: 960–9.

Bradley KM, O'Sullivan VT, Soper ND, Nagy Z, King EM, Smith AD, et al. Cerebral perfusion SPET correlated with Braak pathological stage in Alzheimer's disease. Brain 2002; 125(Pt 8): 1772–81.

Chien DT, Bahri S, Szardenings AK, Walsh JC, Mu F, Su MY, et al. Early clinical PET imaging results with the novel PHF-tau radioligand [F-18]-T807. J Alzheimers Dis 2013; 34: 457–68.

Choi SR, Golding G, Zhuang Z, Zhang W, Lim N, Hefti F, et al. Preclinical properties of 18F-AV-45: a PET agent for Abeta plaques in the brain. J Nucl Med 2009; 50: 1887–94.

Clark CM, Schneider JA, Bedell BJ, Beach TG, Bilker WB, Mintun MA, et al. Use of florbetapir-PET for imaging beta-amyloid pathology. JAMA 2011; 305: 275–83.

Corder EH, Ghebremedhin E, Taylor MG, Thal DR, Ohm TG, Braak H. The biphasic relationship between regional brain senile plaque and neurofibrillary tangle distributions: modification by age, sex, and APOE polymorphism. Ann N Y Acad Sci 2004; 1019: 24–8.

Crane PK, Carle A, Gibbons LE, Insel P, Mackin RS, Gross A, et al. Development and assessment of a composite score for memory in the Alzheimer's Disease Neuroimaging Initiative (ADNI). Brain Imaging Behav 2012; 6: 502–16.

Damoiseaux JS, Seeley WW, Zhou J, Shirer WR, Coppola G, Karydas A, et al. Gender modulates the APOE epsilon4 effect in healthy older adults: convergent evidence from functional brain connectivity and spinal fluid tau levels. J Neurosci 2012; 32: 8254–62.

Fodero-Tavoletti MT, Okamura N, Furumoto S, Mulligan RS, Connor AR, McLean CA, et al. 18F-THK523: a novel *in vivo* tau imaging ligand for Alzheimer's disease. Brain 2011; 134: 1089–100.

Gibbons LE, Carle AC, Mackin RS, Harvey D, Mukherjee S, Insel P, et al. A composite score for executive functioning, validated in Alzheimer's Disease Neuroimaging Initiative (ADNI) participants with baseline mild cognitive impairment. Brain Imaging Behav 2012; 6: 517–27.

Hardy J, Selkoe DJ. The amyloid hypothesis of Alzheimer's disease: progress and problems on the road to therapeutics. Science 2002; 297: 353–6.

Hayasaka S, Du A-T, Duarte A, Kornak J, Jahng G-H, Weiner MW, et al. A non-parametric approach for co-analysis of multi-modal brain imaging data: application to Alzheimer's disease. Neuroimage 2006; 30: 768–79.

Hurtado DE, Molina-Porcel L, Iba M, Aboagye AK, Paul SM, Trojanowski JQ, et al. A{beta} accelerates the spatiotemporal progression of tau pathology and augments tau amyloidosis in an Alzheimer mouse model. Am J Pathol 2010; 177: 1977–88.

Hyman B, Trojanowski J. Consensus recommendations for the postmortem diagnosis of Alzheimer's disease: the National Institute on Aging and Reagan Institute Working Group on diagnostic criteria for the neuropathological assessment of Alzheimer's disease. J Neuropathol Exp Neurol 1997; 56: 1095–7.

Jack CR, Bernstein MA, Fox NC, Thompson P, Alexander G, Harvey D, et al. The Alzheimer's disease neuroimaging initiative (ADNI): MRI methods. J Magn Reson Imaging 2008; 27: 685–91.

Jack CR Jr, Knopman DS, Jagust WJ, Petersen RC, Weiner MW, Aisen PS, et al. Tracking pathophysiological processes in Alzheimer's disease: an updated hypothetical model of dynamic biomarkers. Lancet Neurol 2013; 12: 207–16.

Jagust WJ, Bandy D, Chen K, Foster NL, Landau SM, Mathis CA, et al. The Alzheimer's disease neuroimaging initiative positron emission tomography core. Alzheimers Dement 2010; 6: 221–9.

Johnson KA, Schultz A, Betensky RA, Becker JA, Sepulcre J, Rentz D, et al. Tau positron emission tomographic imaging in aging and early Alzheimer disease. Ann Neurol 2016; 79: 110–9.

Karran E, Mercken M, De Strooper B. The amyloid cascade hypothesis for Alzheimer's disease: an appraisal for the development of therapeutics. Nat Rev Drug Discov 2011; 10: 698–712.

Knopman DS, Parisi JE, Salviati A, Floriach-Robert M, Boeve BF, Ivnik RJ, et al. Neuropathology of cognitively normal elderly. J Neuropathol Exp Neurol 2003; 62: 1087–95.

Landau SM, Fero A, Baker SL, Koeppe R, Mintun M, Chen K, et al. Measurement of longitudinal beta-amyloid change with 18F-florbetapir PET and standardized uptake value ratios. J Nucl Med 2015; 56: 567–74.

Landau SM, Marks SM, Mormino EC, Rabinovici GD, Oh H, O'Neil JP, et al. Association of lifetime cognitive engagement and low beta-amyloid deposition. Arch Neurol 2012; 69: 623–29.

Le Cao K-A, Martin P, Robert-Granie C, Besse P. Sparse canonical methods for biological data integration: application to a cross-platform study. BMC Bioinformatics 2009; 10: 34.

Lin KA, Doraiswamy PM. When Mars versus Venus is not a Cliché: gender differences in the neurobiology of Alzheimer's disease. Front Neurol 2014; 5: 288.

Lo RY, Jagust WJ. Effect of cognitive reserve markers on Alzheimer pathologic progression. Alzheimer Dis Assoc Disord 2013; 27: 343–50.

Markesbery WR. Neuropathological criteria for the diagnosis of Alzheimer's disease. Neurobiol Aging 1997; 18 (Suppl 4): S13–9.

Marquie M, Normandin MD, Vanderburg CR, Costantino IM, Bien EA, Rycyna LG, et al. Validating novel tau positron emission tomography tracer [F-18]-AV-1451 (T807) on postmortem brain tissue. Ann Neurol 2015; 78: 787–800.

Mintun MA, LaRossa GN, Sheline YI, Dence CS, Lee SY, Mach RH, et al. [11C]PIB in a nondemented population: potential antecedent marker of Alzheimer disease. Neurology 2006; 67: 446–52.

Monsell SE, Mock C, Roe CM, Ghoshal N, Morris JC, Cairns NJ, et al. Comparison of symptomatic and asymptomatic persons with Alzheimer disease neuropathology. Neurology 2013; 80: 2121–9.

Mufson EJ, Malek-Ahmadi M, Perez SE, Chen K. Braak staging, plaque pathology, and APOE status in elderly persons without cognitive impairment. Neurobiol Aging 2016; 37: 147–53.

Nelson PT, Braak H, Markesbery WR. Neuropathology and cognitive impairment in Alzheimer disease: a complex but coherent relationship. J Neuropathol Exp Neurol 2009; 68: 1–14.

Payami H, Grimslid H, Oken B, Camicioli R, Sexton G, Dame A, et al. A prospective study of cognitive health in the elderly (Oregon Brain Aging Study): effects of family history and apolipoprotein E genotype. Am J Hum Genet 1997; 60: 948–56.

Petersen RC, Aisen PS, Beckett LA, Donohue MC, Gamst AC, Harvey DJ, et al. Alzheimer's Disease Neuroimaging Initiative (ADNI): clinical characterization. Neurology 2010; 74: 201–9.

Pooler AM, Polydoro M, Maury EA, Nicholls SB, Reddy SM, Wegmann S, et al. Amyloid accelerates tau propagation and toxicity in a model of early Alzheimer's disease. Acta neuropathologica communications 2015; 3: 14.

Price JL. Diagnostic criteria for Alzheimer's disease. Neurobiol Aging 1997; 18 (Suppl 4): S67–70.

Price JL, Morris JC. Tangles and plaques in nondemented aging and "preclinical" Alzheimer's disease. Ann Neurol 1999; 45: 358–68.

Raj A, Kuceyeski A, Weiner M. A network diffusion model of disease progression in dementia. Neuron 2012; 73: 1204–15.

Raj A, LoCastro E, Kuceyeski A, Tosun D, Relkin N, Weiner M. Network diffusion model of progression predicts longitudinal patterns of atrophy and metabolism in Alzheimer's disease. Cell Rep 2015; 10: 359–69.

Savva GM, Wharton SB, Ince PG, Forster G, Matthews FE, Brayne C. Age, neuropathology, and dementia. N Engl J Med 2009; 360: 2302–9.

Scholl M, Lockhart SN, Schonhaut DR, O'Neil JP, Janabi M, Ossenkoppele R, et al. PET imaging of tau deposition in the aging human brain. Neuron 2016; 89: 971–82.

Serrano-Pozo A, Qian J, Monsell SE, Betensky RA, Hyman BT. APOEepsilon2 is associated with milder clinical and pathological Alzheimer disease. Ann Neurol 2015; 77: 917–29.

Sharp ES, Gatz M. Relationship between education and dementia: an updated systematic review. Alzheimer Dis Assoc Disord 2011; 25: 289–304.

Silbert L, Erten-Lyons D, Kaye J, Tran H, Stanfield S, Quinn J, et al. Alzheimer's disease pathology burden associated with clinical dementia decreases with age. Alzheimers Dement 2012; 8: P446.

Stern Y. Cognitive reserve in ageing and Alzheimer's disease. Lancet Neurol 2012; 11: 1006–12.

Terry RD, Katzman R. Senile dementia of the Alzheimer type. Ann Neurol 1983; 14: 497–506.

Terry RD, Masliah E, Hansen LA. The neuropathology of Alzheimer's disease and the structural basis of its cognitive alterations. In: Terry RD, Katzman R, Bick KL, Sisodia SS, editors. Alzheimer's disease. . 1999. pp. 187–206.

Tiraboschi P, Sabbagh MN, Hansen LA, Salmon DP, Merdes A, Gamst A, et al. Alzheimer disease without neocortical neurofibrillary tangles: "a second look". Neurology 2004; 62: 1141–7.

Tustison NJ, Cook PA, Klein A, Song G, Das SR, Duda JT, et al. Large-scale evaluation of ANTs and FreeSurfer cortical thickness measurements. Neuroimage 2014; 99: 166–79.

Vemuri P, Weigand SD, Przybelski SA, Knopman DS, Smith GE, Trojanowski JQ, et al. Cognitive reserve and Alzheimer's disease biomarkers are independent determinants of cognition. Brain 2011; 134Pt 5): 1479–92.

Vemuri P, Whitwell JL, Kantarci K, Josephs KA, Parisi JE, Shiung MS, et al. Antemortem MRI based STructural Abnormality iNDex (STAND)-scores correlate with postmortem Braak neurofibrillary tangle stage. Neuroimage 2008; 42: 559–67.

Villain N, Chételat G, Grassiot B, Bourgeat P, Jones G, Ellis KA, et al. Regional dynamics of amyloid-β deposition in healthy elderly, mild cognitive impairment and Alzheimer's disease: a voxelwise PiB–PET longitudinal study. Brain 2012; 135: 2126.

Weiner MW, Veitch DP, Aisen PS, Beckett LA, Cairns NJ, Cedarbaum J, et al. 2014 Update of the Alzheimer's disease neuroimaging initiative: a review of papers published since its inception. Alzheimers Dement 2015; 11: e1–120.

Witten DM, Tibshirani R, Hastie T. A penalized matrix decomposition, with applications to sparse principal components and canonical correlation analysis. Biostatistics 2009; 10: 515–34.

Wong DF, Rosenberg PB, Zhou Y, Kumar A, Raymont V, Ravert HT, et al. *In vivo* imaging of amyloid deposition in Alzheimer disease using the radioligand 18F-AV-45 (florbetapir [corrected] F 18). J Nucl Med 2010; 51: 913–20.

Xia CF, Arteaga J, Chen G, Gangadharmath U, Gomez LF, Kasi D, et al. [(18)F]T807, a novel tau positron emission tomography imaging agent for Alzheimer's disease. Alzheimers Dement 2013; 9: 666–76.